ACI MATERIALS JOURNAL TECHNICAL PAPER

Title No. 118-M90

Limestone Calcined Clay Cement for Three-Dimensional-Printed Engineered Cementitious Composites

by He Zhu, Kequan Yu, Wesley McGee, Tsz Yan Ng, and Victor C. Li

The feasibility of three-dimensional (3D)-printable (3DP) engineered cementitious composites (ECC) has previously been demonstrated. However, the high carbon footprint of ordinary portland cement-based ECC remains a sustainability challenge. An emerging green limestone calcined clay cement was employed as an intrinsic rheology modifier. Both fresh and hardened properties were investigated. The lower-carbon cement increased the viscosity and shape-retention ability compared to portland cement-based ECC, endowing the new composite with intrinsic printability. The compressive strength and split tensile strength exhibited anisotropy, depending on the loading direction relative to the layered geometry. Despite the negative impact of the progressive cavity pump on fiber dispersion, 3D-printable limestone calcined clay cement-based ECC retained a ductility of 3.0% at 28 days, showing promise in sustainable construction applications.

Keywords: engineered cementitious composites (ECC); fiber; limestone calcined clay cement (LC3); rheology; shape retention; strain-hardening; three-dimensional (3D) print.

INTRODUCTION

Extrusion-based three-dimensional printing (3DP) of concrete is attractive in construction due to its advantages such as increased design flexibility, cost benefits (labor, formwork, material, time), as well as sustainability (low waste and low carbon and energy footprints).[1,2] However, the inherent incompatibility between the concrete extruding process and steel reinforcement required due to the brittle nature of concrete remains a challenge for 3DP concrete applications.[3] Engineered cementitious composites (ECC), self-reinforced with fibers and possessing a strain-hardening behavior, have been demonstrated in full-scale structures and used in repair applications.[2,4] The self-reinforced characteristic of ECC[5,6] promises to overcome the incompatibility between concrete and steel reinforcement in 3DP construction.

The ductility of 3DP-ECC is influenced by fiber dispersion, governed by both material rheology and the extrusion process. The rheological behavior of ECC must satisfy requirements of fiber dispersion, pumpability, printability, and buildability. The challenge is to keep fibers from clumping after extrusion to maintain robust strain-hardening. 3DP-ECC using polyethylene (PE) fiber with high ductility (>3%) has been previously developed.[7,8] However, the high cost of PE fiber limits the use of 3DP-PE-ECC. Polyvinyl alcohol (PVA) fiber, with costs approximately half of PE fiber,[9] has demonstrated robust strain-hardening performance with excellent ability to control crack width in typical ECC. Thus it remains the most used fiber in ECC.[4] Although high strain capacity (>3%) of PVA-ECC has been obtained through manual printing,[5,10,11] the ductility of full-scale 3DP-PVA-ECC elements remains below 0.5%,[12,13] offsetting the performance value of ECC. Further research is needed on the development of 3DP-PVA-ECC with at least 2% tensile ductility.

Limestone calcined clay cement (LC3), usually incorporating clinker, calcined clay, limestone, and gypsum, is gaining popularity due to its low carbon footprint, low embodied energy, and wide availability. Compared to ordinary portland cement (OPC) concrete, LC3 concrete exhibits comparable strength performance and is more durable.[14,15] Additionally, LC3 increases the yield stress, thixotropy, plastic viscosity, and cohesion of concrete.[16] The rheological performance has also been proven to be superior for 3D printing of concrete.[17] LC3 has been used in ECC with more than 30 MPa compressive strength and 6% tensile ductility.[18,19] However, adding fibers to the matrix may present challenges of printability, buildability, and robust strain-hardening of ECC. Thus, it is necessary to investigate the rheological property and mechanical performance of LC3-ECC for 3DP applications.

This research aims to develop a 3D-printable ECC using LC3 and PVA fiber. The goal is to achieve superior rheological behavior and sufficient mechanical performance for 3DP applications. A flow table test per ASTM C1437[20] and a shape retention ability test were conducted to characterize the fresh properties. Anisotropic mechanical properties were investigated by compressive and split tensile strength tests with different loading directions. Finally, the uniaxial tensile ductility was examined.

RESEARCH SIGNIFICANCE

LC3-ECC has been demonstrated as a low-carbon and low-embodied-energy construction material. LC3 holds promises in 3DP applications, including the advantages of enhanced yield stress, thixotropy, plastic viscosity, and cohesion of concrete. This work represents the first demonstration of fresh LC3-ECC as having intrinsic properties suitable for 3DP without the need for additional thixotropic or viscosity control. The development of a 3D-printable LC3-ECC with superior printability, buildability, and ultra-high ductility

ACI Materials Journal, V. 118, No. 6, November 2021.
MS No. M-2020-430.R2, doi: 10.14359/51733109, received April 6, 2021, and reviewed under Institute publication policies.

Table 1—Chemical compositions of OPC, FA, and MK (mass %)

Material	CaO	Al_2O_3	SiO_2	SO_3	Fe_2O_3	MgO	Others
OPC	63.5	4.8	19.6	2.6	2.9	2.2	4.4
FA	17.4	19.8	39.4	1.9	11	3.70	6.8
MK	0.0	46.6	50.8	0.1	0.5	0.0	2.0

Note: Limestone (LS) is highly pure $CaCO_3$ powder, and main composition is CaO.

Table 2—Properties of PVA fiber

Fiber diameter, μm	Length, mm	Young's modulus, GPa	Surface oil content, wt. %	Elongation, %	Nominal strength, MPa	Density, kg/m^3
39	8	42.8	1.2	6.0	1600	1300

will increase the sustainability of the material and construction process.

EXPERIMENTAL INVESTIGATION

Materials

The LC3 cement employed in this study was blended by weight of 55% OPC (Type I), 30% metakaolin (MK), and 15% limestone (LS). Lower-cost, less-pure calcined clays are commonly used in practice. LC3-based concrete with lower-grade MK showed comparable mechanical and durability performance as OPC-based concrete.[21-24] The high-purity MK used in this study was based on laboratory availability to emulate the LC3.

Fly ash (FA) was adopted to tailor the matrix for robust strain-hardening behavior. The adoption of FA in ECC has been demonstrated with ultra-high volume (up to 85%),[25] local source FA,[26,27] different FA types (fineness and CaO contents),[28,29] and even solid waste FA.[30] Although coal-fired power generation is on a decline, coal power is expected to remain a primary power source for the next few decades and will continue to produce FA as a by-product. The current use percentage of FA is just above 50%. Further, FA stored as a landfill can be exploited,[30] suggesting an abundant supply of FA.[31,32] The adoption of FA with a weight ratio of 2.2 to OPC in this study also increases the material greenness.

Table 1 lists the chemical compositions of binder ingredients (OPC, MK, LS, FA), the particle size distribution of which can be found in Zhu et al.[33] High-range water-reducing admixture (HRWR) was obtained. The PVA was used for reinforcement of ECC, as well as a rheology modifier for 3D printing. The properties of micro PVA fibers are listed in Table 2.

ECC mixing process

The dry ingredients (OPC, MK, LS, FA) were pre-mixed for 10 minutes following the weight ratio listed in Table 3. Then, water associated with HRWR was added and further mixed for 10 minutes at 100 RPM to obtain a homogeneous paste. PVA fibers (2% volume) were added to the fresh materials and mixed at 200 RPM for an additional 6 minutes. Mechanical performance tests were conducted for the fresh ECC (Table 4). It should be noted that the ECC for the flow table test, shape retention test and cube samples were prepared in 10 L batches, in a 28.4 L mixer (H30), while the ECC used for 3DP were prepared in 20 L batches, in a 56.8 L mixer (H60). To understand the influence of batch volume on tensile performance of ECC, both H30 and H60 were used in preparing dogbone samples for the uniaxial tensile test.

Table 3—Mixture ratios of mixtures, kg/m^3

Mixture	OPC	MK	LS	FA	Water	HRWR	PVA
OPC-ECC	490	0	0	1077	392	4	26
LC3-ECC	270	147	73	1077	392	4	26
LC3-M	270	147	73	1077	392	4	0

Note: OPC is ordinary portland cement; MK is metakaolin; LS is limestone; FA is fly ash; HRWR is high-range water-reducing admixture; and PVA is polyvinyl alcohol.

Table 4—Experimental protocol

Mixture	Flow table	Shape retention	Cast			3DP		
			f_c	f_t	f_{spl}	f_c	f_t	f_{spl}
OPC-ECC	×	×	×	×	×	—	—	—
LC3-ECC	×	×	×	×	×	×	×	×
LC3-M	×	×	—	—	—	—	—	—

Note: × is measured items; – is not measured items; f_c, f_t, and f_{spl} represents compressive strength, uniaxial tensile strength, and split tensile strength, respectively.

Fresh property test

Rheology control is crucial for 3DP-ECC. Flowability (important for material transport from the mixer to extruder and for extrusion) was measured using the flow table test per ASTM C1437.[20] The end of ECC mixing marked time zero, and flow table tests were conducted at 20-, 40-, 60-, and 80-minute increments. The spread diameter results were calculated by the average value of the maximum spread diameter (d_1) and its perpendicular diameter (d_2), as illustrated in Fig. 1(a). These measurements were taken after 25 drops of the flow table each.

The shape retention capacity is important for ECC printing as layers need to support consecutive layers overlaid on top without deformation.[8] High shape retention is necessary for layers' buildability to ensure the success of the outcome. An evaluation method for shape retention was developed herein based on previous studies.[8,34] As shown in Fig. 1(b), the ECC/mortar cake was produced by a plastic mold measuring 60 mm in diameter and 13 mm in height. A plastic plate was then gently placed on top of the fresh mixture to distribute the pressure uniformly. Weights of different mass were added carefully, and a caliper was employed to monitor the height of the ECC/mortar cake (Fig. 1(b)). The ratio of the difference in height relative to the original was adopted as the shape retention index. The weight corresponding to 80 and 50% of height ratio, indicating the maximum allowable weight of consecutive printing and layer buckling, was measured at 20, 40, 60, and 80 minutes.

3DP-ECC and mechanical performance test

After mixing, the fresh ECC was placed into a hopper mounted on a servo-driven peristaltic pump. Due to the inherent pulsation of the peristaltic pump, feeding with a stable flow rate for printing proved difficult. To achieve a more consistent flow rate, ECC was transported by a 4 m hose to a custom-built servo-driven progressive cavity pump

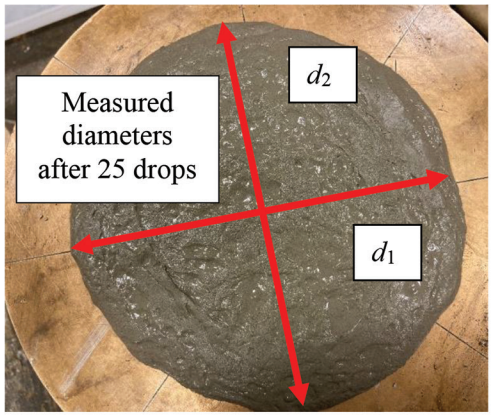

(a) Flow table test.

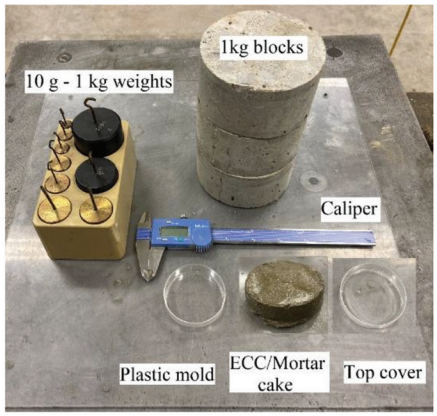

(b) The tools for shape retention test.

Fig. 1—Flow table test.

mounted at the end of the robotic arm (Fig. 2). The progressive cavity pump can feed material with highly linear flow rates in relation to pump speed.[2,35] The ECC was extrusion-printed through customized nozzles onto a foam board in specific patterns to produce samples for various tests (Fig. 3).

The ECC was printed with a U-turn shape with six segments of usable filaments between the turns. The dimension of each segment measures 50 mm in width, 600 mm in length, and 10 mm in thickness. Three days after printing, the segments (Fig. 3(a)) were sawn into 50 mm cubes for the compressive test. Compression load was applied in perpendicular and parallel directions relative to the printed layer (Fig. 4). Due to the limitation of fabricating 3DP cylinder specimens, 50 mm cubes were adopted for investigating the anisotropy of split tensile strength (Fig. 5), where D1, D2, and D3 indicated that the loading bar was parallel to, perpendicular to, and along with the printed layers, respectively. Because ECC is a strain-hardening material, the measured split tensile strength was calculated with the ultimate peak load rather than at first crack[36] using Eq. (1)[37]

$$f_{split} = \frac{2P_{max}}{\pi A}\left(1-\left(\frac{b}{H}\right)^2\right)^{\frac{3}{2}} \quad (1)$$

where P_{max} and A are the ultimate peak load and loading section areas. The strip width-height ratio (b/H) was 1/6 as suggested by Carmona[38] to obtain a measured split tensile strength with lower size dependency. The uniaxial tensile test was performed along the printing direction (Fig. 3(b)). ECC was printed with a 30 mm width, 13 mm thickness, and 800 mm length filament, where 300 mm length filament was sawn off for testing. The sawn filament was placed in the dogbone mold (Fig. 6(b)), and the rest of the mold was then filled with cast ECC to form the ends of the dogbone. Besides the 3DP samples, mold-cast ECC was also prepared for compression, split tension, and direct tension tests for comparison. The uniaxial tensile test was not conducted in a direction normal to the print direction. Yu et al.[11] found that 3DP-ECC showed a tension-softening behavior in a direction normal to the interfacial planes because very few

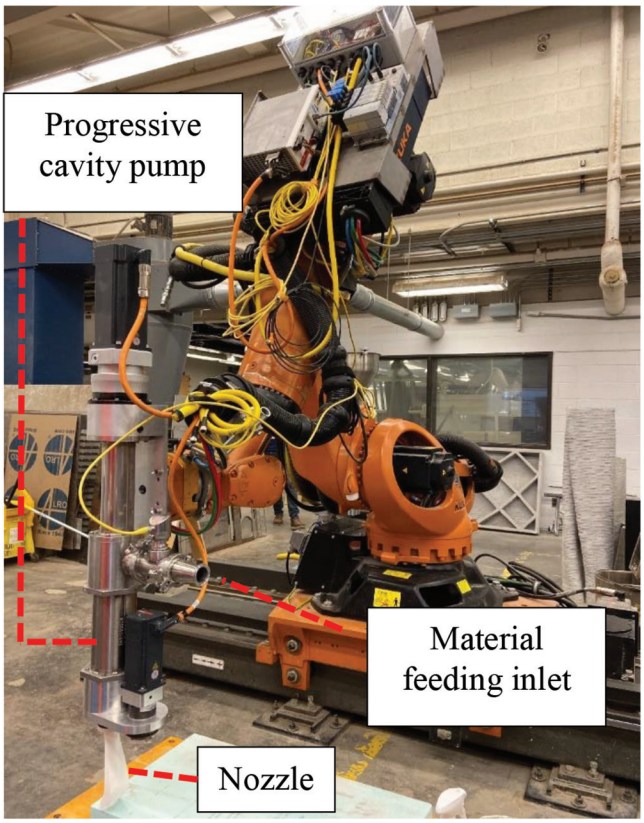

Fig. 2—3D printing system.

fibers cross adjacent layers. This test was not repeated in the current study.

The specimens were cured at room temperature at 20 ± 3°C, 40 ± 5% relative humidity (RH), and tested at 3, 7, and 28 days. Three cubes (50 x 50 x 50 mm) per batch were used for the compressive test per ASTM C109,[39] and six cubes were employed for split tensile tests. Three mold-cast (Fig. 6(a)) and six 3DP dogbone-shaped specimens (Fig. 6(b)) per mixture were performed on a servo-hydraulic system at a rate of 0.5 mm/min for direct tensile tests. The deformation was measured by two linear variable displacement transducers (LVDT) with an 80 mm gauge length (Fig. 6(c)).

(a) 3DP LC3-ECC for compressive and split tensile tests (Printed with six layers of filaments by 50 mm width, 600 mm length, and 10 mm thickness).

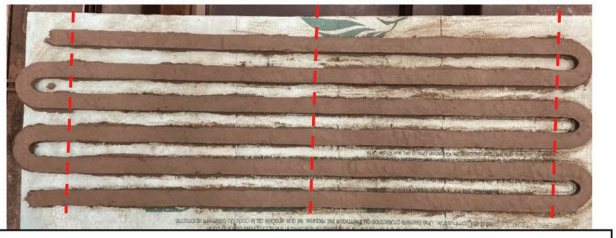

(b) 3DP LC3-ECC for the direct tensile test (Printed with one layer of the filament by 30 mm width, 800 mm length, and 13 mm thickness).

Fig. 3—3DP LC3-ECC for making cubes and dogbone specimens.

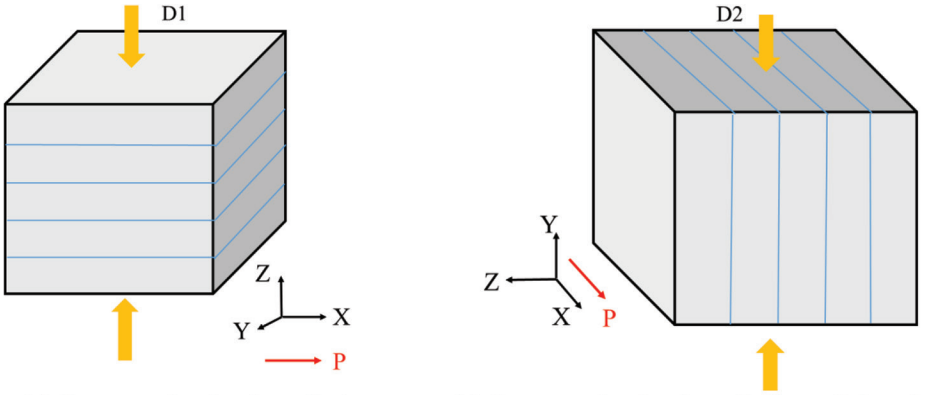

(a) Compressive load applied perpendicularly to the printed layers.

(b) Compressive load applied parallel to the printed layers.

Fig. 4—Compressive strength of 3DP LC3-ECC with different loading directions.

The crack numbers after tensioning were counted within the gauge length (80 mm). The average crack width was calculated by dividing the tensile strain capacity by crack number and multiplying the gauge length. The average crack space was obtained by dividing the gauge length by the crack number.

EXPERIMENTAL RESULTS

Fresh properties

The influence of LC3 cement and PVA fibers on the rheology of ECC was investigated by the flowability and shape retention ability (Fig. 7). The flow table test (Fig. 7(a)) data indicate that the spread diameter of OPC-ECC is larger than those of LC3-ECC and LC3-M (mortar without fiber). During the first 60 minutes, OPC-ECC spread across the entire drop table given the HRWR content, with the diameter of the flow table at 260 mm. At 80 minutes, the spread diameter of the OPC-ECC dropped to 240 mm. By replacing the OPC with LC3, the flowability of the fresh paste decreased notably. The initial spread diameter of LC3-M was 220 µm at 5 minutes. The addition of PVA fibers reduced the initial spread diameter of LC3-ECC to 170 µm. As expected, the flowability of LC3-ECC decreased with time, and the spread diameter at 80 minutes was only 135 mm. Because the flowability below 130 mm would increase the risk of blockage for the extruder, the time window for printing was set as 80 minutes in this study.

The shape retention ability of LC3-ECC is significantly higher than LC3-M (Fig. 7(b)), indicating the considerable influence of the PVA fibers' addition. Typically, lag time is necessary between the end of mixing and the beginning of printing. Twenty minutes is usually sufficient for most practical applications.[4] The bearable weight of 80% shape retention is 1.7 kg for LC3-ECC at 20 minutes, which is 2.4 times that of LC3-M (Fig. 8(a) and (b)). The ECC/mortar cake's self-weight is approximately 60 g, indicating that the initial

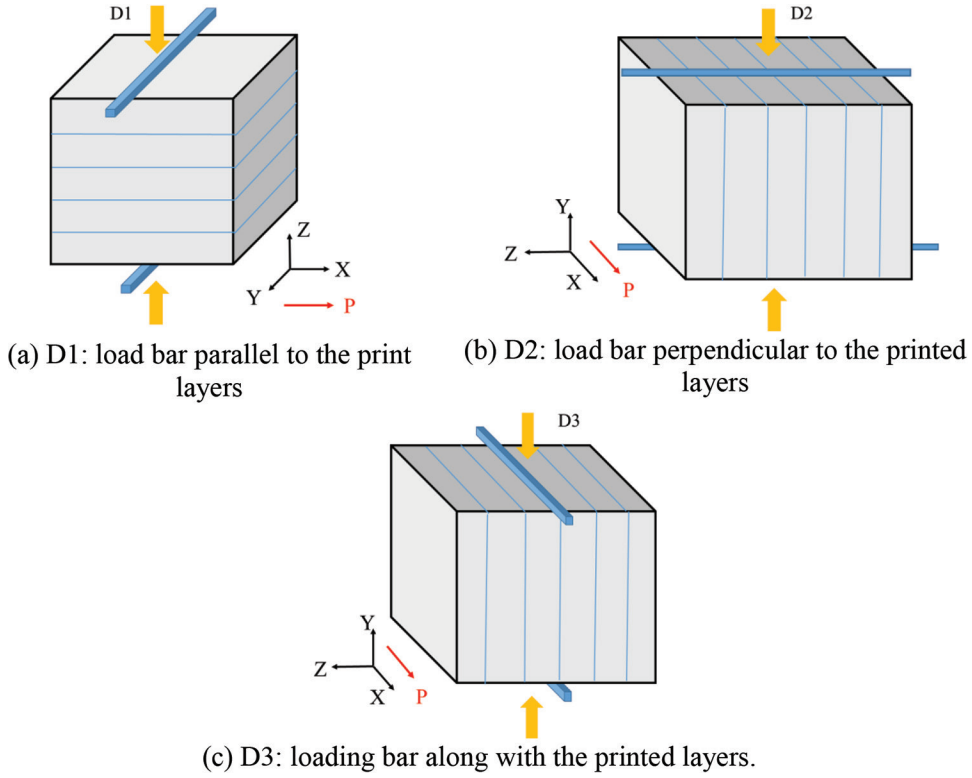

(a) D1: load bar parallel to the print layers

(b) D2: load bar perpendicular to the printed layers

(c) D3: loading bar along with the printed layers.

Fig. 5—Split tensile test of 3DP LC3-ECC with different loading directions.

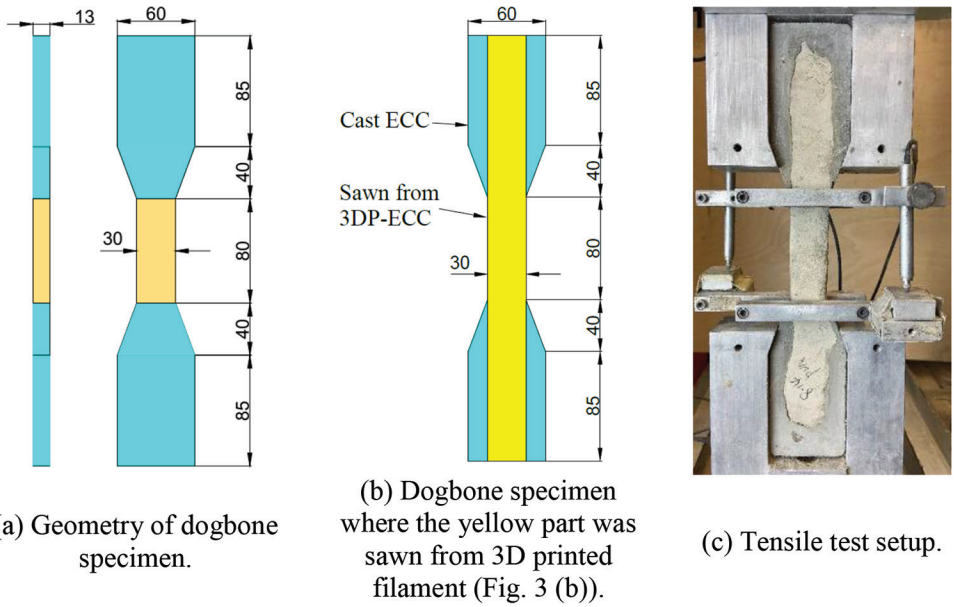

(a) Geometry of dogbone specimen.

(b) Dogbone specimen where the yellow part was sawn from 3D printed filament (Fig. 3 (b)).

(c) Tensile test setup.

Fig. 6—Uniaxial tensile specimens and setup.

allowable printed layer of LC3-ECC could be built up to 28 layers at 20 minutes. The bearable weight augments with time, and the weight of 80% shape retention of LC3-ECC is 7.0 kg (Fig. 8(c)), while for LC3-M, it is 4.0 kg. The maximum buildup layers could be 117 for LC3-ECC at 80 minutes. The bottom layer of LC3-ECC could hold 80% of its original height if the layer build speed were to be controlled to below 26 mm/min. The freestanding weight can be further increased if the allowable height deformation is relaxed. However, the height retention ratio is suggested to be higher than 50%, below which the printed filaments are prone to buckling failure. Figure 7(b) plots the maximum allowable weight corresponding to 50% shape retention or buckling condition, suggesting an upper limit of the print speed. The addition of PVA fiber significantly enhances the material's shape retention ability, which further increases the allowable layer build speed of printing.

Compressive strength

Figure 9 shows the compressive strength development with curing age. The compressive strength of cast-LC3-ECC is lower than cast-OPC-ECC at early age. However, the compressive strength of cast-LC3-ECC at 33.5 MPa is comparable with that of cast-OPC-ECC at 36 MPa at 28 days. Although

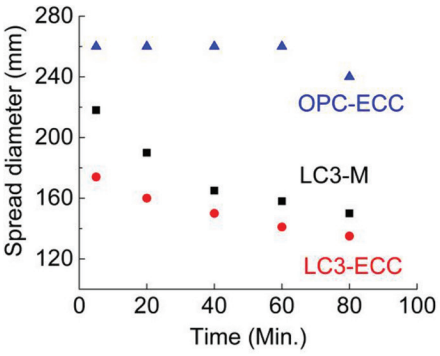

(a) The flowability versus time.

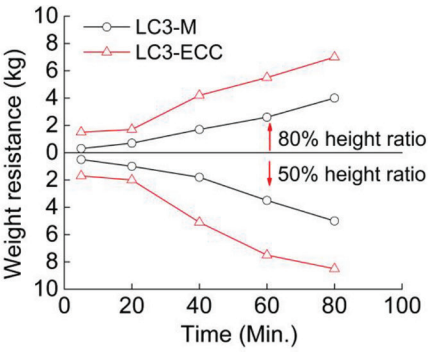

(b) Maximum allowable weight corresponding to 80% or 50 % shape retention ability.

Fig. 7—Fresh properties of ECC and mortar.

(a) Bulge-deformation of LC3-M with 1 kg weight at 20 min.

(b) LC3-ECC retained 80% of the original height with 1 kg weight at 20 min.

(c) LC3-ECC retained 80% of the original height with 7 kg weight at 80 min.

Fig. 8—Shape retention ability of LC3-ECC and mortar.

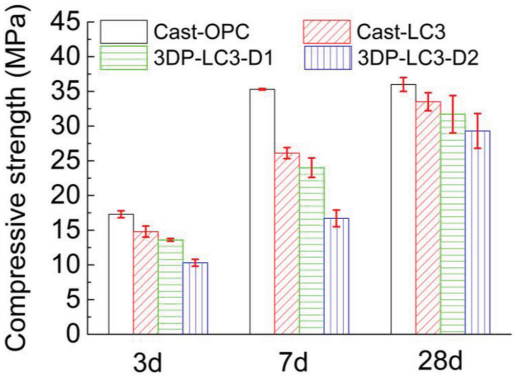

Fig. 9—Compressive strength of cast and 3DP ECC.

LC3-ECC (55% OPC, 30% MK, 15% LS) has a lower OPC content in comparison with OPC-ECC, continuous strength gain is observed, reflecting the pozzolanic effect of MK.[19,33]

The 3DP cubes exhibit anisotropic compressive strength (Fig. 9). The compressive strength ratio of 3DP-LC3-D1 to cast-LC3 ECC is 91, 91, and 95% at 3, 7, and 28 days, respectively. The compressive strength in the D2 direction (loading direction parallel to the printed layers, Fig. 4(b)) is notably weaker than the mold cast-LC3 before 7 days. The compressive strength of 3DP-LC3-D2 is 10.3 MPa at 3 days and 16.7 MPa at 7 days, corresponding to 69% and 64% of the compressive strength of mold cast-LC3 ECC at the same age. However, 3DP-LC-D2 experienced a significant strength increase at 28 days (29.3 MPa), more than 1.7 times that of 7 days, amounting to 87% compressive strength of the mold cast-LC3 ECC at 28 days. Compressive strength decay along the printed layer direction has also been reported in the literature,[17,34,40] attributed to the weakening effect of a higher porosity in the printed layers. A larger variability of the 3DP cubes than the mold cast cubes is observed.

Instead of brittle fractures observed in concrete, cast-LC3 ECC cubes (Fig. 10(a)) exhibit multiple microcracks after peak loading. The subparallel cracks are bridged by fibers and controlled in width, mostly below 100 µm. In addition to the vertical cracks, some horizontal cracks between layers are observed for 3DP-LC3-D1 (Fig. 10(b)). In contrast, only a few cracks are found along with the printed layers of 3DP-LC3-D2 (Fig. 10(c)), indicating that the interface between printed layers influences the stress path and the compressive strength of 3DP-D2 cubes.

(a) Cast-LC3 (b) 3DP-LC3-D1 (c) 3DP-LC3-D2

Fig. 10—Compression failure mode of cast and 3DP ECC at 28 days.

Split tensile strength

Figure 11 shows the development of split tensile strength with curing age. The 3-day split tensile strength of 3DP-LC3-D1 and 3DP-LC3-D2 is 2.9 and 2.3 MPa, respectively, amounting to 111% and 88% of the cast-LC3 ECC at 2.7 MPa. At 28 days, 3DP-LC3-D1 shows a slightly higher split tensile strength than cast-LC3, while 3DP-LC3-D2 and 3DP-LC3 have comparable split tensile strengths.

As expected, the split tensile strength between printed layers (D3 direction) is significantly lower than the cast-LC3 ECC and 3DP-LC3 ECC in D1 and D2 directions. The ratio of 3DP-LC3-D3 to cast-LC3 is approximately 1/3 at 3 days, increasing to 1/2 at 28 days. However, the split tensile strength gain over time of 3DP-LC3-D3 is faster, showing a similar trend to the compressive strength gain.

Figure 12 shows the failure mode after the split tensile test for cast and 3DP ECC. For cast-LC3, multiple microcracks are found distributed along the tensile stress axis between the loading bars (Fig. 12(a)). In addition to the microcracks along the tensile stress axis, horizontal cracks between printed layers can be observed with the 3DP-LC3-D1 specimen (Fig. 12(b)), accounting for the slightly higher split tensile strength than cast-LC3. The failure mode in the D2 direction is quite different from the D1 direction. In addition to the microcracks on the front surface, some macro cracks were observed on the side surface. The crack number on the side surface decreases with curing age (Fig. 12(d), (e), and (f)). The cracks on the side surface are affected by the interfaces between printed layers. Weaker bonding induces more cracks at an early age when compared with fewer cracks at 28 days.

Although multiple cracks are observed in cast-LC3 ECC and 3DP-LC3 in D1 and D2 directions, only a few macro cracks can be observed along with the printed layers (Fig. 12(c)), reflecting the brittle nature of the interfaces. PVA fibers are distributed along the print direction in the printed layers, while few fibers bridge the layers. The brittle interface between layers remains a vital issue for 3DP ECC; the 3DP-ECC structure should be carefully designed to avoid excessive tensile stress across layers.

Uniaxial tensile performance

The uniaxial tensile test results of the cast and 3DP ECC are shown in Fig. 13. Similar to the compressive strength, the tensile strength of the H30-cast-LC3 is lower than that of the H30-cast-OPC at early age but are comparable at 28 days (Fig. 13(a)). Although the OPC-binder ratio of LC3-ECC

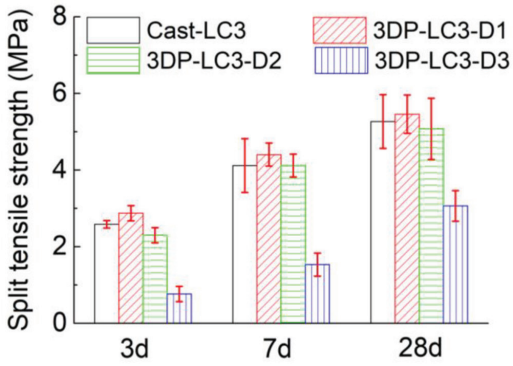

Fig. 11—Split tensile strength of cast and 3DP ECC.

is lower than OPC-ECC, LC3 ECC exhibits sufficient strength increase at a later age. Unlike the tensile strength results of OPC-ECC, the average tensile strain capacity of the H30-cast-LC3 is 6.3% at 3 days, much larger than that of H30-cast-OPC (4.5%). The ductility of H30-cast-LC3 decreases with curing time and is 4.4% at 28 days, similar to that of H30-cast-OPC (4.6%). The strength and ductility development of cast-LC3 ECC are in accordance with the finding in Zhang et al.[19] In summary, the developed LC3-ECC has comparable tensile strength and ductility to the OPC-ECC at 28 days.

The ultimate tensile strength (Fig. 13) is comparable to the split tensile strength (Fig. 11) for the cast specimens. For concrete and fiber-reinforced concrete (FRC), the split tensile strength to direct tensile strength ratio reported in the literature[36,41-44] reveals a large range (102 to 200%), depending on the specimen details (size, geometry, and compositions) and test conditions (setup and curing history). This difference between ECC and plain concrete/FRC reflects the different failure mechanisms of these material classes. The ductile failure of ECC is governed by the fiber bridging stress, while plain concrete and FRC exhibit brittle or quasi-brittle fracture so that the tensile strength is dominated by matrix conditions (flaw size and matrix fracture toughness). In contrast, the ultimate tensile strength and the split tensile strength in ECC reflect the maximum fiber bridging stress determined by fiber and fiber/matrix interface properties.

Fiber dispersion uniformity critically affects the tensile ductility of ECC. ECC prepared with different mixers may result in different tensile performances. 3DP applications usually require a larger volume of materials than specimen testing. Therefore, the influence of mixer size or batch size in relation to tensile strength and ductility was investigated

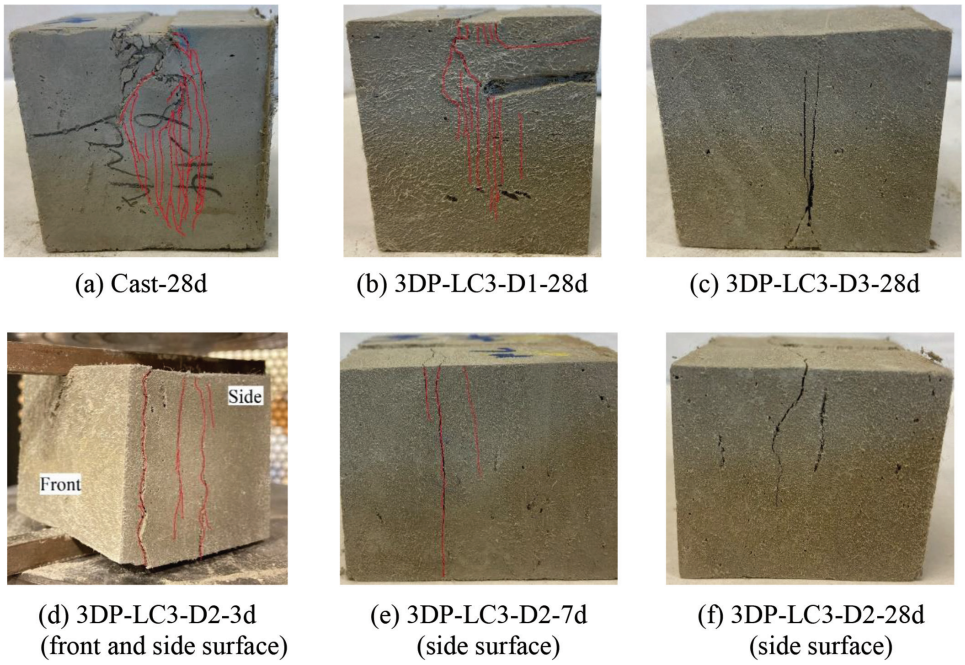

(a) Cast-28d (b) 3DP-LC3-D1-28d (c) 3DP-LC3-D3-28d

(d) 3DP-LC3-D2-3d (front and side surface) (e) 3DP-LC3-D2-7d (side surface) (f) 3DP-LC3-D2-28d (side surface)

Fig. 12—Failure mode of split tensile test.

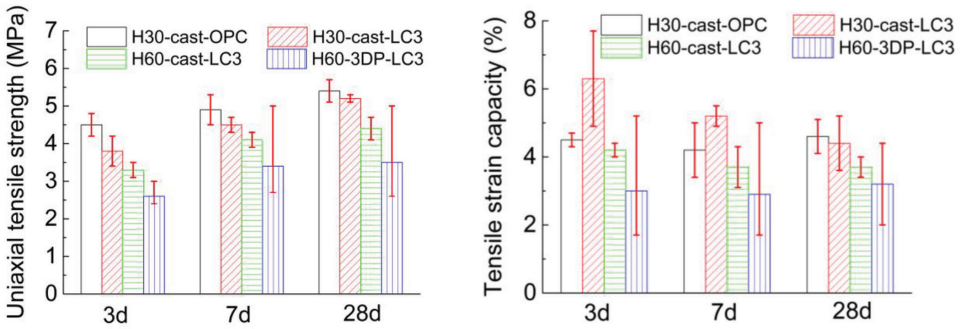

(a) Uniaxial tensile strength (b) Tensile strain capacity

Fig. 13—Uniaxial tensile results of cast and 3DP ECC at 3, 7, and 28 days.

using two mixers, H30 and H60. Figure 13 shows that H60 batches have reduced tensile strength and strain capacity compared to the ECC cast by H30 mixing. The H60-3DP-LC3 has a tensile strength of 4.4 MPa and a tensile strain capacity of 3.7%, compared to 5.2 MPa and 4.4% of H30-3DP-LC3 at 28 days. The performance degradation due to different mixer use was also reported by Lepech et al.[45] The fiber dispersion of large-scale mixing is not as uniform as small-scale mixing (affected by the volume, speed, and power of the mixer).

The dogbone specimens typically fail by fracture localization on the plane with the least amount of fibers. However, in the split tensile cubes, the least fiber section may differ from the loading section. Hence, the weakest section in the 3DP dogbone specimens shows a lower ultimate tensile strength compared to the split tensile strength.

Comparing the effect of 3DP versus cast processing, the tensile performance of H60-3DP-LC3 is diminished compared to H60-cast-LC3 (Fig. 13). The average uniaxial tensile strength decreases from 4.4 MPa to 3.5 MPa at 28 days, and a 20% uniaxial tensile strength loss can be observed after printing. The average tensile strain capacity of 3DP-LC3 ECC maintains approximately 3.0% from 3 to 28 days. Although the reduced tensile performance is found in 3DP-LC3 ECC, the average tensile strength at 3.5 MPa and strain capacity at 3.0% remain comparable to those of 3DP ECC reported in the literature.[5,8,10,11] Larger variability of the tensile results is observed compared to traditional cast specimen in the uniaxial tensile stress-strain response of 3DP-LC3 ECC (Fig. 13 and 14) and nozzle-cast-LC3 ECC (Fig. 15), as reported in previous studies.[5,10] The large errors of 3DP specimens are caused by non-uniform fiber dispersions affecting the printing process.

Table 5 summarizes the cracking characteristics of the dogbone specimens after tension tests. The average crack width of the H30-cast-OPC ECC is 57.3 μm, and the average crack spacing is 1.3 mm at 28 days, revealing a saturated multiple-cracking pattern (Fig. 16(a)). The crack pattern of H30-cast-OPC ECC is consistent with that of the OPC-ECC from the literature.[4,19] The crack number of H30-cast-LC3 is 32, compared to 65 of H30-cast-OPC ECC, where the crack width and spacing are approximately twice that of H30-cast-OPC ECC. The crack patterns of cast-LC3-ECC prepared by different mixers (H30 and H60) are not significantly different. The crack number and spacing of the

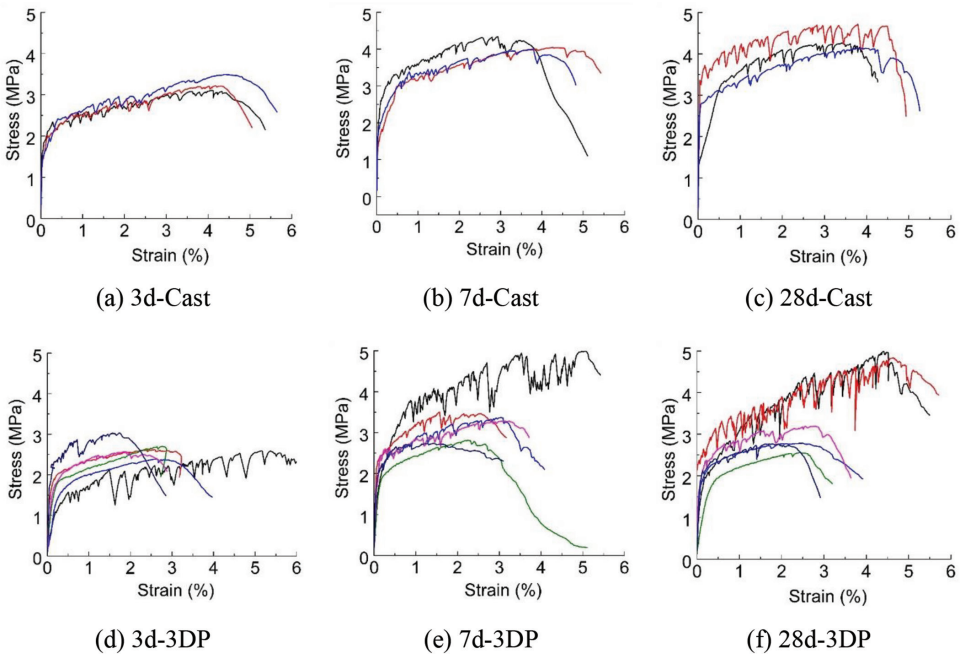

Fig. 14—Uniaxial tensile stress-strain curves of cast/3DP LC3-ECC at 3, 7, and 28 days.

H60-3DP-LC3 were almost the same as H60-cast-LC3; however, the crack width corresponding to the maximum tensile strength of the H60-3DP-LC3 is significantly reduced, leading to the lower strain capacity of the printed specimen.

Additional flaws were found in the 3DP samples compared to the cast specimen, as shown in Fig. 12(b) and 17(c), which has also been reported in other 3DP studies.[13,40] Flaws promote crack formation and propagation; hence, more cracks were induced at a relatively low-stress level for 3DP-LC3, accounting for the small crack width in 3DP specimens.

DISCUSSION

Extruding system and fiber dispersion

The diminished tensile performance and higher variability observed limit the advantage of 3DP-ECC. The underlying reasons were investigated in this study. It appears that fiber clumping, as revealed on the fracture surface of 3DP-LC3 ECC (Fig. 17(d) and (e)) dogbone specimens, is the main cause.

The printing process plays a major role in fiber dispersion uniformity. Different from mold-cast ECC, the 3DP ECC was pumped by a peristaltic pump after mixing, delivered through the hose, then extruded by a progressive cavity pump through a customized nozzle (Fig. 2). Because ECC has been demonstrated to work well with peristaltic pumps to deliver the material through a hose in spray applications,[46,47] the fiber dispersion problem is most likely a result of the material processed through the progressive cavity pump which was used to moderate pulsation caused by the peristaltic pump.

To investigate the effect of the extruding process, fresh ECC materials were collected after extrusion from the nozzle and then cast directly into the dogbone mold, labeled as nozzle-cast-LC3 ECC. The tensile stress-strain response of the nozzle-cast-LC3 ECC (Fig. 15) shows apparent variability, similar to 3DP-LC3 ECC (Fig. 14).

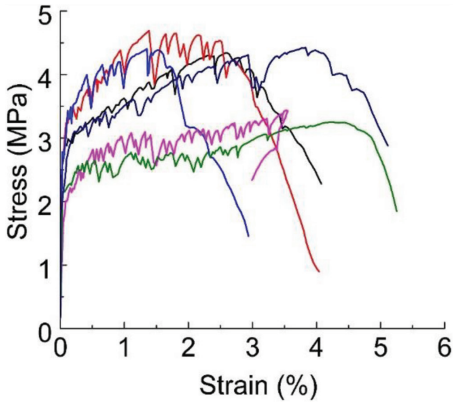

Fig. 15—Twenty-eight-day uniaxial tensile stress-strain relationship of the nozzle-cast-LC3 ECC (fresh ECC was collected and cast after extruded out of nozzle).

The ECC was extruded out from the narrow gap between the stator and rotor of the progressive cavity pump (several millimeters). The internal geometry of the progressive cavity pump, including the gap dimension and extruding length, influenced fiber dispersion, which negatively impacts the tensile strain-hardening of ECC. One cracked specimen of nozzle-cast-LC3 ECC (Fig. 17(e)) showed fewer fibers than H60-LC3 ECC, indicating non-uniform fiber dispersion after extrusion.

Table 6 summarizes the tensile results of cast-ECC and 3DP-ECC from the literature. Depending on the extruding method, both improved and reduced tensile properties have been reported. While manual extrusion with a caulk gun can achieve a comparable or better tensile performance, the process between the caulk gun and mechanically controlled 3DP is different. For 3DP application using ram-extrusion,[12] only 0.5% tensile ductility was obtained, much lower than this study. Apart from PVA fiber, 3DP ECC with PE fiber demonstrated good performance with both auger-extrusion method[7] and progressive cavity pump-extrusion,[8] likely due

Table 5—Average crack number, width, and space after uniaxial tensile tests

Mixture	3 days			7 days			28 days		
	No.	CW, μm	Crack space, mm	No.	CW, μm	Crack space, mm	No.	CW, μm	Crack space, mm
H30-cast-OPC	52 (2)	69.1 (1.7)	1.5 (0.1)	56 (4)	56.7 (3.9)	1.4 (0.1)	65 (10)	57.3 (8.5)	1.3 (0.2)
H30-cast-LC3	37 (4)	133.3 (8.2)	2.2 (0.3)	37 (3)	105.1 (20.2)	2.2 (0.2)	32 (1)	111.7 (10.7)	2.5 (0.1)
H60-cast-LC3	39 (4)	68 (8.4)	2.1 (0.2)	36 (1)	80.8 (13.2)	2.2 (0.1)	37 (2)	95.6 (8.2)	2.2 (0.1)
H60-3DP-LC3	38 (5)	64.5 (5.4)	2.2 (0.3)	39 (7)	67.8 (6.3)	2.1 (0.4)	37 (6)	59.8 (6.4)	2.2 (0.3)

Note: No. is number of cracks; CW is crack width; and number in parentheses is standard deviation of corresponding parameters.

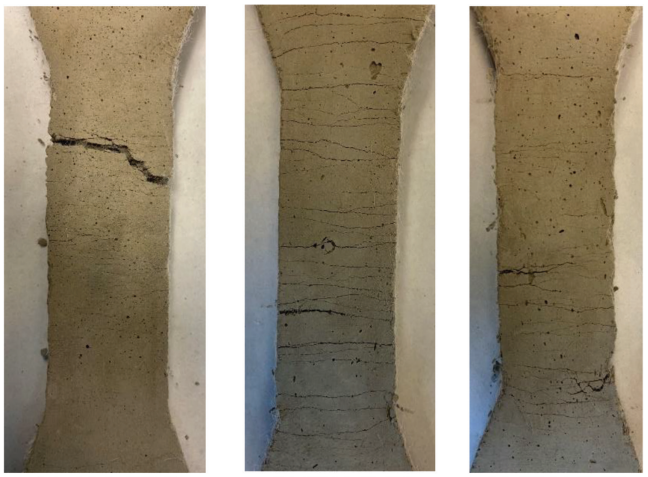

(a) 28d-OPC (b) H30-LC3 (c) H60-LC3

Fig. 16—Crack patterns of cast specimens after tension test.

to the high strength of PE fibers, which can produce robust tensile strain-hardening[48] with lower fiber content (1.5%).

Sample quality

Apart from fiber dispersion, test sample quality is another factor that may affect the measured tensile performance. Although the rheology of LC3-ECC was deliberately designed for 3DP printing in terms of extrusion and buildability, the low flowability of 3DP-ECC leads to more air void in the printed sample, which has been found in Chaves et al.[13] and also shown in Fig. 12(b) and 17(c). In the 13 mm thickness tensile dogbone specimen, large defects caused by incomplete compaction of the low flowability 3DP ECC may lead to unsaturated cracking and local failure (Fig. 17(b)).

CONCLUSIONS

Three-dimensional-printable (3DP) engineered cementitious composites (ECC) have been developed using limestone calcined clay cement (LC3) and polyvinyl alcohol (PVA) fiber. Fresh and hardened properties were systematically investigated. The following conclusions can be drawn:

1. The flowability of LC3-ECC was significantly lower than that of ordinary portland cement and engineered cementitious composites (OPC-ECC) with the same water reducer content. Despite the lower cement content, LC3-ECC attained 28 days of compressive strength, tensile strength, and tensile ductility comparable to OPC-ECC. The advantages of lowered embodied carbon increased viscosity and superior mechanical performance, making LC3-ECC an attractive material for 3DP.

2. In addition to the effect of mechanical reinforcement, PVA fiber was found to act as a viscosity modifier in the fresh state. The addition of 2% volume of PVA fiber significantly enhanced the shape retention ability of the fresh composite.

3. The printed LC3-ECC exhibited anisotropic compressive and split tensile strength, which was significantly impacted by printed layer interfaces. The 3DP-LC3 ECC has comparable 28-day-strengths compared to cast-LC3 ECC for D1-compression, D1-split tension, and D2-split tension direction. The strengths of D2-compression and D3-split tension are lower than the cast specimens.

4. Mixer capacity and material volume were found to influence the quality of fiber dispersion, affecting the tensile strain-hardening performance of ECC. These factors should be considered for large-scale 3DP applications of ECC.

5. The narrow gap between the stator and rotator of the progressive cavity pump promoted fiber clumping, accounting for the large variability of tensile strength and ductility of 3DP-ECC specimens. Additional research is needed to overcome this limitation. Despite this, the developed 3DP-LC3 ECC retains an average tensile strength of 3.5 MPa and ultra-high strain capacity of 3.0% at 28 days.

AUTHOR BIOS

He Zhu *is a Postdoctoral Research Fellow at the Department of Civil and Environmental Engineering at the University of Michigan, Ann Arbor, MI. He received his PhD from Tsinghua University, Beijing, China. His research interests include the sustainability of engineered cementitious composites (ECC), rheology control of ECC (spray, three-dimensional [3D] printing, and normal cast), the infrastructure repair, low shrinkage/self-stressing ECC, and restrained cracking of concrete.*

Kequan Yu *is a Postdoctoral Research Fellow at the University of Michigan. He received his PhD from Tongji University, Shanghai, China, and The Hong Kong Polytechnic University, Hung Hom, Hong Kong. His research interests include the development of high-strength, high-ductility concrete (HSHDC) and its application in structural engineering, covering both the material and structural element fields.*

Wesley McGee *is the Co-founder and Partner of Matter Design. He is currently an Associate Professor and the Fabrication and Robotics Lab Director at the University of Michigan. His research interests include the innovation in design and fabrication across a range of material processes, particularly in the application of industrial robotic tools to architectural production.*

Tsz Yan Ng *is the Principal of an independent architecture and art practice with built works in the United States and China. She serves as Assistant Professor of architecture at the University of Michigan. Her research interests are collaborative in nature and interdisciplinary in scope and range in scale from textile manufacturing facilities to commercial retail interiors or installations.*

Victor C. Li, *FACI, is an E. Benjamin Wylie Collegiate Professor of Civil Engineering and James R. Rice Distinguished University Professor of Engineering at the University of Michigan. His research interests include*

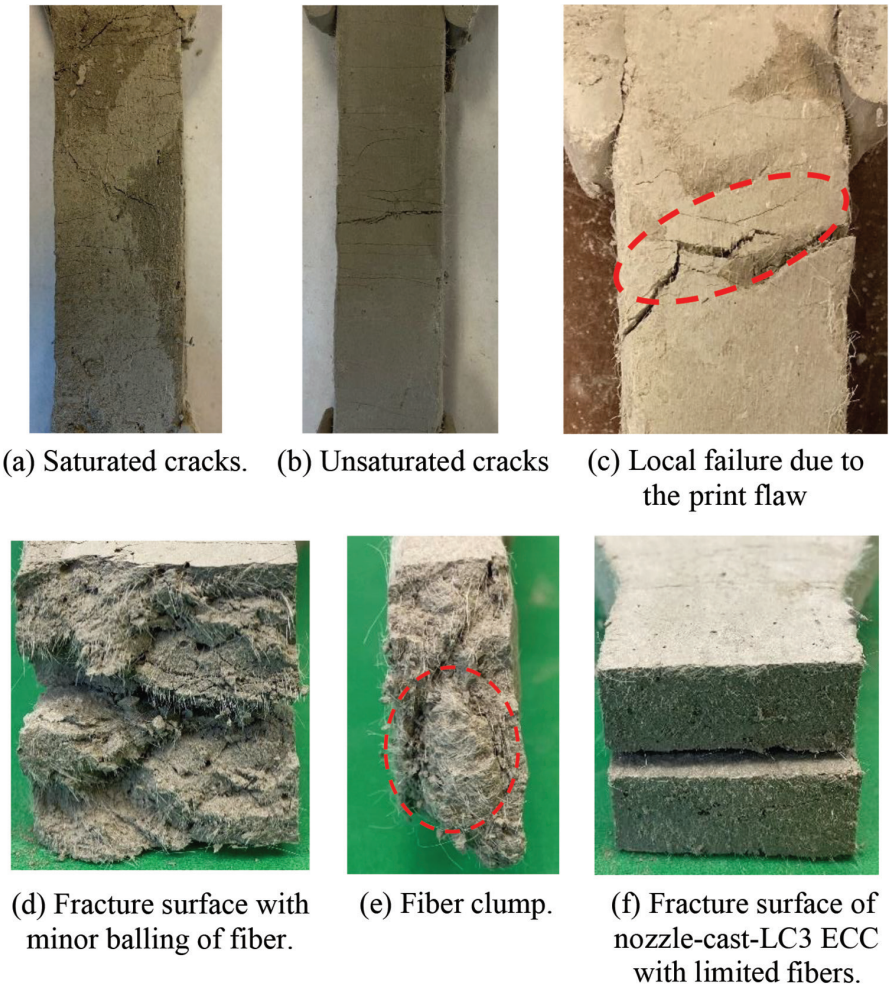

Fig. 17—Crack patterns of 3DP specimens after tension test.

Table 6—Comparison of cast-ECC and 3DP-ECC in literature

Reference	Extruder	Fiber	C-f_t (MPa)	C-ε_t, %	3DP-f_t, MPa	3DP-ε_t, %
Soltan and Li[5]	Caulk gun	PVA	~2.8*	~1.7*	~4.0	~2.9
Bao and Li[10]	Caulk gun	PVA	5.6	3.6	5.5	3.1
Yu et al.[11]	Caulk gun	PVA	3.2	4.0	3.5	5.1
Chaves et al.[12]	Ram-extrusion	PVA	—	—	< 2.5	< 0.5
Ogura et al.[8]	Progressive cavity pump	1.5% HDPE	6.3	1.7	5.7	3.2
Zhu et al.[7]	Auger-type extruder	2% HDPE	5.0	10.0	5.3	11.4
		1.5% HDPE	5.0	8.5	5.7	9.6

*Results of cast and 3DP samples were based on coupon specimen, while tensile strength and ductility of dogbone-shaped specimen with same mixture were approximately 6 MPa and 3.5%.
Note: C-f_t and C-ε_t represent ultimate tensile strength and ductility of cast specimen; 3DP-f_t and 3DP-ε_t represent ultimate tensile strength and ductility of 3DP specimen.

designing, processing, and characterizing smart fiber-reinforced cementitious composites for resilient and sustainable built environments.

ACKNOWLEDGMENTS

This research is partially supported by the Center for Low Carbon Built Environment (CLCBE) at the University of Michigan and the University of Michigan MCubed 3.0 Program, and the UM CoE Theme and Cluster Program. Material donations from BORAL RESOURCES (fly ash) are gratefully acknowledged.

REFERENCES

1. Ma, G.; Wang, L.; and Ju, Y., "State-Of-The-Art Of 3D Printing Technology of Cementitious Material—An Emerging Technique for Construction," *Science China Technological Sciences*, V. 61, No. 4, 2018, pp. 475-495. doi: 10.1007/s11431-016-9077-7

2. Li, V. C.; Bos, F. P.; Yu, K.; McGee, W.; Ng, T. Y.; Figueiredo, S. C.; Nefs, K.; Mechtcherine, V.; Nerella, V. N.; Pan, J.; van Zijl, G. P. A. G.; and Kruger, P. J., "On The Emergence of 3D Printable Engineered, Strain Hardening Cementitious Composites (ECC/SHCC)," *Cement and Concrete Research*, V. 132, 2020, p. 106038. doi: 10.1016/j.cemconres.2020.106038

3. Mechtcherine, V.; Bos, F. P.; Perrot, A.; da Silva, W. R. L.; Nerella, V. N.; Fataei, S.; Wolfs, R. J. M.; Sonebi, M.; and Roussel, N., "Extrusion-Based Additive Manufacturing with Cement-Based Materials–Production Steps, Processes, and Their Underlying Physics: A Review," *Cement and Concrete Research*, V. 132, 2020, p. 106037. doi: 10.1016/j.cemconres.2020.106037

4. Li, V. C., *Engineered Cementitious Composites (ECC)*, Springer, New York, 2019.

5. Soltan, D. G., and Li, V. C., "A Self-Reinforced Cementitious Composite for Building-Scale 3D Printing," *Cement and Concrete Composites*, V. 90, 2018, pp. 1-13. doi: 10.1016/j.cemconcomp.2018.03.017

6. Yu, K.; Li, L.; Yu, J.; Xiao, J.; Ye, J.; and Wang, Y., "Feasibility of Using Ultra-High Ductility Cementitious Composites for Concrete

Structures Without Steel Rebar," *Engineering Structures*, V. 170, 2018, pp. 11-20. doi: 10.1016/j.engstruct.2018.05.037

7. Zhu, B.; Pan, J.; Nematollahi, B.; Zhou, Z.; Zhang, Y.; and Sanjayan, J., "Development of 3D Printable Engineered Cementitious Composites with Ultra-High Tensile Ductility for Digital Construction," *Materials & Design*, V. 181, 2019, p. 108088. doi: 10.1016/j.matdes.2019.108088

8. Ogura, H.; Nerella, V. N.; and Mechtcherine, V., "Developing and Testing of Strain-Hardening Cement-Based Composites (SHCC) in the Context of 3D-Printing," *Materials (Basel)*, V. 11, No. 8, 2018, p. 1375. doi: 10.3390/ma11081375

9. Zhang, D.; Yu, J.; Wu, H.; Jaworska, B.; Ellis, B. R.; and Li, V. C., "Discontinuous Micro-Fibers as Intrinsic Reinforcement for Ductile Engineered Cementitious Composites (ECC)," *Composites Part B: Engineering*, V. 184, 2020, p. 107741. doi: 10.1016/j.compositesb.2020.107741

10. Bao, Y.; Xu, M.; Soltan, D.; Xia, T.; Shih, A.; Clack, H.; and Li, V. C., "Three-Dimensional Printing Multifunctional Engineered Cementitious Composites (ECC) for Structural Elements." International RILEM Conference on Concrete and Digital Fabrication, Springer, 2018, pp. 115-28.

11. Yu, J., and Leung, C. K. Y., "Impact of 3D Printing Direction on Mechanical Performance of Strain-Hardening Cementitious Composite (SHCC)." RILEM International Conference on Concrete and Digital Fabrication. Springer, 2018. pp. 255-65.

12. Figueiredo, S. C.; Rodríguez, C. R.; and Ahmed, Z. Y., "An Approach to Develop Printable Strain Hardening Cementitious Composites," *Materials & Design*, V. 169, 2019, p. 107651. doi: 10.1016/j.matdes.2019.107651

13. Figueiredo, S. C.; Rodríguez, C. R.; Ahmed, Y., Z.; Bos, D. H.; Xu, Y.; Salet, T. M.; Copuroglu, O.; Schlangen, E.; and Bos, F. P., "Mechanical Behavior of Printed Strain Hardening Cementitious Composites," *Materials*, V. 13, No. 10, 2020, p. 2253.

14. Scrivener, K.; Martirena, F.; Bishnoi, S.; and Maity, S., "Calcined Clay Limestone Cements (LC3)," *Cement and Concrete Research*, V. 114, 2018, pp. 49-56. doi: 10.1016/j.cemconres.2017.08.017

15. Dhandapani, Y., Sakthivel, T., Santhanam, M., et al. "Mechanical Properties and Durability Performance of Concretes with Limestone Calcined Clay Cement (LC3)," *Cement and Concrete Research*, V. 107, July 2017, pp. 136-51.

16. Muzenda, T. R.; Hou, P.; Kawashima, S.; Sui, T.; and Cheng, X., "The Role of Limestone and Calcined Clay on the Rheological Properties of LC3," *Cement and Concrete Composites*, V. 107, 2020, p. 103516. doi: 10.1016/j.cemconcomp.2020.103516

17. Chen, Y.; Figueiredo, S. C.; Li, Z.; Chang, Z.; Jansen, K.; Çopuroğlu, O.; and Schlangen, E., "Improving Printability of Limestone-Calcined Clay-Based Cementitious Materials by Using Viscosity-Modifying Admixture," *Cement and Concrete Research*, V. 132, 2020, p. 106040. doi: 10.1016/j.cemconres.2020.106040

18. Zhu, H.; Zhang, D.; Wang, T.; Wu, H.; and Li, V. C., "Mechanical and Self-Healing Behavior of Low Carbon Engineered Cementitious Composites Reinforced With PP-Fibers," *Construction and Building Materials*, V. 259, 2020, p. 119805. doi: 10.1016/j.conbuildmat.2020.119805

19. Zhang, D.; Jaworska, B.; Zhu, H.; Dahlquist, K.; and Li, V. C., "Engineered Cementitious Composites (ECC) With Limestone Calcined Clay Cement (LC3)," *Cement and Concrete Composites*, V. 114, 2020, p. 103766. doi: 10.1016/j.cemconcomp.2020.103766

20. ASTM C1437-15, "Standard Test Method for Flow of Hydraulic Cement Mortar," ASTM International, West Conshohocken, PA, 2015.

21. Avet, F., and Scrivener, K., "Investigation of the Calcined Kaolinite Content on the Hydration of Limestone Calcined Clay Cement (LC3)," *Cement and Concrete Research*, V. 107, Jan. 2018, pp. 124-135. doi: 10.1016/j.cemconres.2018.02.016

22. Maraghechi, H., Avet, F., Wong, H., Kamyab, H.; and Scrivener, K., "Performance of Limestone Calcined Clay Cement (LC3) With Various Kaolinite Contents With Respect to Chloride Transport," *Materials and Structures/Materiaux et Constructions*, V. 51, No. 5, 2018, pp. 1-17.

23. Zhao, D., and Khoshnazar, R., "Microstructure of Cement Paste Incorporating High Volume of Low-Grade Metakaolin," *Cement and Concrete Composites*, V. 106, 2020, p. 103453.

24. Badogiannis, E., and Tsivilis, S., "Exploitation of Poor Greek Kaolins: Durability of Metakaolin Concrete," *Cement and Concrete Composites*, V. 31, No. 2, 2009, pp. 128-133. doi: 10.1016/j.cemconcomp.2008.11.001

25. Yang, E. H.; Yang, Y.; and Li, V. C., "Use of High Volumes of Fly Ash to Improve ECC Mechanical Properties and Material Greenness," *ACI Materials Journal*, V. 104, No. 6, Nov.-Dec. 2007, pp. 620-628.

26. Ma, H., Qian, S., Zhang, Z., Lin, Z.; and Li, V., "Tailoring Engineered Cementitious Composites with local ingredients," *Construction and Building Materials*, V. 101, No. Part 1, 2015, pp. 584-595.

27. Arce, G.; Noorvand, H.; Hassan, M.; and Rupnow, T., "Evaluation of the Performance of Engineered Cementitious Composites (ECC) Produced from Local Materials BT—International Congress on Polymers in Concrete (ICPIC 2018)," Springer, 2018. pp. 181-186.

28. Kan, L.; Shi, R.; and Zhu, J., "Effect of Fineness and Calcium Content of Fly Ash on The Mechanical Properties of Engineered Cementitious Composites (ECC)," *Construction and Building Materials*, V. 209, 2019, pp. 476-484. doi: 10.1016/j.conbuildmat.2019.03.129

29. Ma, H.; Qian, S.; and Li, V. C., "Influence of Fly Ash Type on Mechanical Properties and Self-Healing Behavior of Engineered Cementitious Composite (ECC)," *Materials Science*, 2016.

30. Kan, L.; Shi, R.; Zhao, Y.; Duan, X.; and Wu, M., "Feasibility Study on Using Incineration Fly Ash From Municipal Solid Waste to Develop High Ductile Alkali-Activated Composites," *Journal of Cleaner Production*, V. 254, 2020, p. 120168. doi: 10.1016/j.jclepro.2020.120168

31. Assi, L. N.; Carter, K.; Deaver, E.; and Ziehl, P., "Review of Availability of Source Materials for Geopolymer/Sustainable Concrete," *Journal of Cleaner Production*, V. 263, 2020, p. 121477. doi: 10.1016/j.jclepro.2020.121477

32. Diaz-Loya, I.; Juenger, M.; Seraj, S.; and Minuteskara, R., "Extending Supplementary Cementitious Material Resources: Reclaimed and Remediated Fly Ash and Natural Pozzolans," *Cement and Concrete Composites*, V. 101, 2019, pp. 44-51. doi: 10.1016/j.cemconcomp.2017.06.011

33. Zhu, H.; Zhang, D.; Wang, T.; Wu, H.; and Li, V. C., "Mechanical and Self-Healing Behavior of Low Carbon Engineered Cementitious Composites Reinforced With PP-Fibers," *Construction and Building Materials*, V. 259, 2020, p. 119805. doi: 10.1016/j.conbuildmat.2020.119805

34. Arunothayan, A. R.; Nematollahi, B.; Ranade, R.; Bong, S. H.; and Sanjayan, J., "Development of 3D-Printable Ultra-High Performance Fiber-Reinforced Concrete for Digital Construction," *Construction and Building Materials*, V. 257, 2020, p. 119546. doi: 10.1016/j.conbuildmat.2020.119546

35. McGee, W.; Ng, T. Y.; Yu, K.; and Li, V. C., "Extrusion Nozzle Shaping for Improved 3DP of Engineered Cementitious Composites (ECC/SHCC)," *RILEM International Conference on Concrete and Digital Fabrication*, Springer, 2020. pp. 916-25.

36. Denneman, E., Kearsley, E. P., and Visser, A. T. "Splitting Tensile Test For Fibre Reinforced Concrete," *Materials and Structures/Materiaux et Constructions*, V. 44, No. 8, 2011, pp. 1441-1449.

37. Tang, T., "Effects of Load-Distributed Width on Split Tension of Unnotched and Notched Cylindrical Specimens," *Journal of Testing and Evaluation*, V. 22, No. 5, 1994, pp. 401-409. doi: 10.1520/JTE12656J

38. Carmona, S., and Aguado, A., "New Model for the Indirect Determination of the Tensile Stress-Strain Curve of Concrete by Means of the Brazilian Test," *Materials and Structures*, V. 45, No. 10, 2012, pp. 1473-1485. doi: 10.1617/s11527-012-9851-0

39. ASTM C109/C109M-20b, "Standard Test Method for Compressive Strength of Hydraulic Cement Mortars (Using 2-in. or [50 mm] Cube Specimens)," ASTM International, West Conshohocken, PA, 2020.

40. Chen, Y.; Romero Rodriguez, C.; Li, Z.; Chen, B.; Çopuroğlu, O.; and Schlangen, E., "Effect of Different Grade Levels of Calcined Clays on Fresh and Hardened Properties of Ternary-Blended Cementitious Materials for 3D Printing," *Cement and Concrete Composites*, V. 114, July 2020.

41. Goaiz, H. A.; Farhan, N. A.; Sheikh, M. N.; Yu, T.; and Hadi, M. N. S., "Experimental Evaluation of Tensile Strength Test Methods for Steel Fibre-Reinforced Concrete," *Magazine of Concrete Research*, V. 71, No. 8, 2019, pp. 385-394. doi: 10.1680/jmacr.17.00516

42. Abrishambaf, A.; Barros, J. A. O.; and Cunha, V. M. C. F., "Tensile Stress-Crack Width Law for Steel Fibre Reinforced Self-Compacting Concrete Obtained from Indirect (Splitting) Tensile Tests," *Cement and Concrete Composites*, V. 57, 2015, pp. 153-165. doi: 10.1016/j.cemconcomp.2014.12.010

43. Zheng, W.; Kwan, A. K. H.; and Lee, P. K. K., "Direct Tension Test of Concrete," *ACI Materials Journal*, V. 98, No. 1, 2001, pp. 63-71.

44. Raphael, J. M., "Tensile Strength of Concrete," *ACI Journal Proceedings*, V. 81, No. 2, Mar.-Apr. 1984, pp. 158-165.

45. Lepech, M. D., and Li, V. C., "Large-Scale Processing of Engineered Cementitious Composites," *ACI Materials Journal*, V. 105, No. 4, July-Aug. 2008, pp. 358-366.

46. Kim, Y. Y.; Kong, H. J.; and Li, V. C., "Design of Engineered Cementitious Composite Suitable for Wet-Mixture Shotcreting," *ACI Materials Journal*, V. 100, No. 6, Nov.-Dec. 2003, pp. 511-518.

47. Zhu, H.; Yu, K.; and Li, V. C., "Sprayable Engineered Cementitious Composites (ECC) Using Calcined Clay Limestone Cement (LC3) and PP Fiber," *Cement and Concrete Composites*, V. 115, 2021, p. 103868. doi: 10.1016/j.cemconcomp.2020.103868

48. Wang, Y.; Liu, F.; Yu, J.; Dong, F.; and Ye, J., "Effect of Polyethylene Fiber Content on Physical and Mechanical Properties of Engineered Cementitious Composites," *Construction and Building Materials*, V. 251, 2020, p. 118917. doi: 10.1016/j.conbuildmat.2020.118917